

The MIN- N family of pure-displacement, triangular, Mindlin plate elements

Y. Jane Liu[†]

*Department of Civil and Environmental Engineering, Tennessee Technological University,
Cookeville, TN 38505-0001, USA*

H. R. Riggs[‡]

*Department of Civil and Environmental Engineering, University of Hawaii at Manoa,
2540 Dole St. Holmes Hall 383, Honolulu, HI 96822, USA*

(Received January 13, 2004, Accepted November 3, 2004)

Abstract. In recent years the pure displacement formulation for plate elements has not been as popular as other formulations. We revisit the pure displacement formulation for shear-deformable plate elements and propose a family of N -node, displacement-compatible, fully-integrated, pure-displacement, triangular, Mindlin plate elements, MIN- N . The development has been motivated by the relative simplicity of the pure displacement formulation and by the success of the existing 3-node plate element, MIN3. The formulation of MIN3 is generalized to obtain the MIN- N family, which possesses complete, fully compatible kinematic fields, in which the interpolation functions for transverse displacement are one degree higher than those for rotations. General element-level formulas for the thin-limit Kirchhoff constraints are developed. The 6-node, 18 degree-of-freedom element MIN6, with cubic displacement and quadratic rotations, is implemented and tested extensively. Numerical results show that MIN6 exhibits good performance for both static and dynamic analyses in the linear, elastic regime. The results illustrate that the fully-integrated MIN6 element has excellent performance in the thin limit, even for coarse meshes, and that it does not require shear relaxation.

Key words: Mindlin plate elements; displacement formulation; triangular plate elements; higher-order plate elements.

1. Introduction

Much of the recent work on plate bending finite elements has focussed on Mindlin plate theory as compared to Kirchhoff plate theory. The primary advantages of Mindlin theory, specifically the inclusion of shear deformation and the low-order (C^0) continuity required for finite element implementations, are well-known. The primary difficulty with Mindlin elements is that 'basic' low-order displacement elements tend to experience shear locking, or at least are excessively stiff, when

[†] Assistant Professor, Corresponding author, E-mail: jliu@ntech.edu

[‡] Professor

modeling thin plates. Shear locking in Mindlin elements results from their inability to satisfy, in the thin limit, the Kirchhoff constraints of vanishing transverse shear strains everywhere within the element without the introduction of additional spurious constraints. Numerous strategies have been used to avoid these problems, such as incompatible modes, discrete penalty constraints; selective, reduced integration; and improved shear strain interpolations (Tessler 1985). A few of the many finite elements based on these approaches are described in (Batoz 1982, Belytschko *et al.* 1984, Choi and Park 1999, Hughes *et al.* 1977, Hughes and Tezduyar 1981, MacNeal 1978, Pugh *et al.* 1978, Sheikh and Dey 2001, Xu 1992).

Of the above techniques to obtain a robust shear-deformable element, the assumed strain technique is currently one of the more popular (Bathe *et al.* 1989, Bathe and Dvorkin 1985, Belytschko and Wong 1989, Brezzi *et al.* 1989, MacNeal 1982, Sze 1997, Sze and Zhu 1998, Zienkiewicz and Lefebvre 1988). Although these elements can have good performance, assumed strain elements can be viewed as a mixed formulation, in which the transverse displacement and rotations are interpolated 'as usual', but transverse shear strains are assumed and interpolated separately. As a result, these formulations are typically more complex than pure displacement elements.

The objective of this paper is to revisit the pure displacement formulation for plate elements and to develop a family of such elements with good performance for both thin and moderately thick plates. One approach that has been used for pure displacement elements to satisfy more readily the Kirchhoff constraints with polynomial interpolation functions is to interpolate the transverse displacement with functions that are one degree higher than the rotations in the thin limit. To achieve this, independent interpolation functions for the transverse displacements and the normal rotations can be used. If this is done, however, one has more degrees-of-freedom for the displacements than the rotations, which can be inconvenient for general applications, and there is therefore motivation to eliminate these 'extra' degrees-of-freedom.

Timoshenko beam theory, the 1-D analog to Mindlin plate theory, has similar problems with shear locking, and the earliest application of independent interpolation with different degrees to solve shear locking was by de Veubeke (1965) for a Timoshenko beam element. He eliminated the 'extra' degrees of freedom for the displacement by static condensation (see also (Crisfield 1986)). Static condensation requires more element computations, and it also reduces the element's application in dynamic analysis. A more elegant approach to eliminate the extra degrees-of-freedom was developed by Tessler and Dong (1981). They started with independently interpolated elements. From these, they developed 'constrained' elements, eliminating the extra DOFs by reducing the order of the shear strain variation in the element. This procedure leads to explicit interpolation functions that can be used to develop pure displacement elements that are fully integrated but that do not lock. The elimination of the extra DOFs result in coupling the transverse displacement field to the rotational DOFs through the interpolation functions.

One of the first applications of independent, different-degree interpolation to Mindlin elements was to rectangular elements by Greimann and Lynn (1970). Hughes and Tezduyar (1981) developed an element that was conceptually based on such an interpolation, although in practice they used equal-degree interpolation functions with a modification of the shear strain to avoid locking. Tessler (Tessler 1982, Tessler and Hughes 1983, 1985) extended his approach for Timoshenko beams to Mindlin plates (the approach and result of which is similar to (Greimann and Lynn 1970) for rectangular plates). He developed the 3-node, 9-DOF 'constrained' element MIN3, with simple, explicit interpolation functions. This fully-integrated, full-rank, low-order (constant moment), pure

displacement element has been shown to perform very well for very thin to moderately thick plates, and it has been extended to shells (Tessler 1990). Crisfield (1984) also used independent interpolations to develop a displacement element. He used similar shear constraints to eliminate some DOFs, but the constrained element actually has more nodes with rotational than displacement degrees-of-freedom.

It should be noted that although the initial elements have independent interpolation, constraints are introduced that couple the transverse displacement field to the rotational degrees-of-freedom. The resulting functions have been referred to in the literature as anisoparametric, interdependent, and linked interpolation functions (Auricchio and Taylor 1994). One could also start with such interpolation functions. This approach has been used to develop mixed Mindlin plate elements (Auricchio and Taylor 1994, Taylor and Auricchio 1993, Xu 1992, Zienkiewicz *et al.* 1993). Mixed elements, however, lack the simplicity of pure displacement elements (as long as the latter require no special procedures to obtain adequate performance).

Of the elements surveyed, only MIN3 (Tessler and Hughes 1985) has the following characteristics: pure-displacement element; simple, explicit, complete polynomial interpolation functions; displacement-compatible; full integration; and good performance for thin and moderately thick plates. The strategy herein is to extend the approach used to develop MIN3 to higher-order elements. First, we review the basic equations of the underlying, linear elastic Mindlin plate theory and the basic concepts of the original MIN3 development. Following that, we present a general methodology to develop interpolation functions for higher-order elements in the MIN-N ‘family’ of N -node, triangular Mindlin elements, in which N is also the number of terms in the complete 2-D polynomial (i.e., 3, 6, 10, etc.) that is used to interpolate the normal rotations. MIN3 is the lowest order element in the family. Then, the approach is used to develop MIN6, a 6-node, 18 DOF, cubic-displacement triangular element. Lastly, we present numerical results for MIN6 and compare them to results for MIN3, for an isoparametric 6-node element (ISOMIN6), and for the 6-node ANSYS element SHELL93 (ANSYS 1998).

2. Basic equations

Consider a plate in the x - y plane with thickness t and mid-plane area A . Let $u(x, y, z)$ and $v(x, y, z)$ be the plate in-plane displacements of a point (x, y, z) and $w(x, y)$ be the transverse displacement of a point (x, y) on the mid-surface of the plate. Let $\theta_x(x, y)$ and $\theta_y(x, y)$ be the rotations about the (negative) x and (positive) y -axes, respectively, of the line that was initially normal to the undeformed midsurface. We assume that plane sections remain plane but not necessarily normal to the deformed midplane. Therefore,

$$u(x, y, z) = z\theta_y(x, y), \quad v(x, y, z) = z\theta_x(x, y) \quad \text{and} \quad w(x, y, z) = w(x, y) \quad (1)$$

The plate bending curvatures and transverse shear strains are, respectively,

$$\boldsymbol{\kappa} = \begin{Bmatrix} \kappa_{xx} \\ \kappa_{yy} \\ \kappa_{xy} \end{Bmatrix} = \begin{Bmatrix} \theta_{y,x} \\ \theta_{x,y} \\ \theta_{y,y} + \theta_{x,x} \end{Bmatrix} \quad \text{and} \quad \boldsymbol{\gamma} = \begin{Bmatrix} \gamma_{xz} \\ \gamma_{yz} \end{Bmatrix} = \begin{Bmatrix} w_{,x} + \theta_y \\ w_{,y} + \theta_x \end{Bmatrix} \quad (2)$$

Given the strain definitions, the moment-curvature relations and shear resultant-strain relations can be written as $\mathbf{M} = \mathbf{D}_b \boldsymbol{\kappa}$ and $\mathbf{Q} = \mathbf{G}_s \boldsymbol{\gamma}$, respectively, where \mathbf{D}_b and \mathbf{G}_s are constitutive matrices. The shear constitutive matrix includes the classical shear correction factor, k^2 (typically 5/6 for a homogeneous plate).

The rotations θ_x , θ_y and the transverse displacement w are considered as independent variables in Mindlin theory. However, in the thin plate limit the Kirchhoff constraints of vanishing shear deformation lead to

$$w_{,x} + \theta_y \rightarrow 0 \quad \text{and} \quad w_{,y} + \theta_x \rightarrow 0 \quad (3)$$

The inability of the interpolated displacement fields of a pure displacement element to satisfy Eq. (3) everywhere within the element leads to shear locking in the thin limit.

In a displacement finite element formulation, the deformations are related kinematically to the displacements such that $\boldsymbol{\kappa} = \mathbf{B}_b \mathbf{d}$ and $\boldsymbol{\gamma} = \mathbf{B}_s \mathbf{d}$, in which \mathbf{d} is the vector of nodal displacements, and \mathbf{B}_b and \mathbf{B}_s are the strain-displacement matrices. Standard theory then leads to the element stiffness matrix, \mathbf{K} , in terms of its bending, \mathbf{K}_b , and transverse shear, \mathbf{K}_s , components:

$$\mathbf{K} = \mathbf{K}_b + \mathbf{K}_s = \int_A \mathbf{B}_b^T \mathbf{D}_b \mathbf{B}_b dA + \int_A \mathbf{B}_s^T \mathbf{G}_s \mathbf{B}_s dA \quad (4)$$

3. MIN3 overview

In this section we review the basic concept and formulation of MIN3. Details of the derivation can be found in Tessler and Hughes (1985). The initial nodal configuration involves 6 nodes: 3 vertex nodes with translational and rotational degrees-of-freedom, and 3 midside nodes with translational degrees-of-freedom only. Note that this strategy is the exact opposite of Hughes' heterosis element (Hughes and Cohen 1978), which involved more nodes with rotational than translational degrees-of-freedom. Standard, triangle interpolation functions are used for the independent interpolation of the displacement variables, which results in a complete quadratic variation for the displacement, a complete linear variation for the rotations, and a complete linear variation for the transverse shear strains. To eliminate the three transverse displacement degrees-of-freedom at the midside nodes while maintaining interelement compatibility, the tangential shear strain along each edge is required to be constant, i.e.,

$$\gamma_{s,z,s} = (w_{,s} + \theta_n)_{,s} \Big|_{\xi_i=0} \equiv 0, \quad i = 1, 2, 3 \quad (5)$$

where s denotes the edge coordinate, θ_n is the rotation normal to the edge, and ξ_i are the usual area coordinates. Enforcement of these constraints leads to a constrained transverse deflection field, in terms of the nine vertex DOFs, that remains a complete quadratic polynomial. However, the shear strain is no longer a complete linear polynomial.

Element matrices follow from standard displacement-based finite element formulation. Full integration is used to evaluate the element stiffness, Eq. (4), and it therefore has full rank.

The different degree interpolation is not sufficient to eliminate locking under all boundary conditions; see Tessler (1985). To eliminate locking completely, Tessler and Hughes (1985)

enhanced the classical shear correction, k^2 , with a finite element relaxation factor, ϕ^2 . That is, k^2 is replaced with $k_e^2 = \phi^2 k^2$. The factor ϕ^2 is calculated automatically. Its maximum value is 1, which corresponds to no relaxation. In the thin limit, as the element thickness approaches zero relative to its size, the factor tends to zero. Another advantage of the relaxation introduced by ϕ^2 is that the excessive stiffness inherent with coarse meshes is reduced.

The success of MIN3 is due to both the interpolation function strategy and the element-appropriate shear relaxation factor. It is a very good element, based upon numerical testing on linear, elasto-static problems.

4. Derivation of the MIN-N family

4.1 General strategy

Because of the displacement basis of MIN3, it is clear that a family of elements can be defined once a methodology is established to generate the interpolation functions. Such a methodology is presented in this section. The desired triangular N -node, $3N$ -DOF elements, MIN- N , must have complete polynomial interpolation for the transverse displacement, w , that is one degree higher than the interpolation of the normal rotations, θ_x and θ_y .

The first step in the derivation is to define a family of unconstrained elements that are based on independent interpolations of the transverse displacement and normal rotations. Standard interpolations for the rotations are used with the usual triangular nodal configuration, as shown in Fig. 1. These interpolation functions have degree $p = (\sqrt{1 + 8N} - 3)/2$. Hierarchical interpolation functions are employed for the higher-order terms of the transverse displacement field. From the unconstrained interpolation functions, the constrained interpolation functions for MIN- N are developed by enforcing continuous shear constraints along any line in the N -node element, which reduces the degree of completeness of the shear strain field by one. As a result of imposing these constraints, the hierarchical (nodeless) DOFs are eliminated and the transverse displacement of the constrained element is then coupled with the rotational degrees-of-freedom. The constrained element has the same nodal configuration, with the same nodal DOF, as the unconstrained element (which also has nodeless DOFs). The displacement fields for the unconstrained and constrained elements are compared in Table 1.

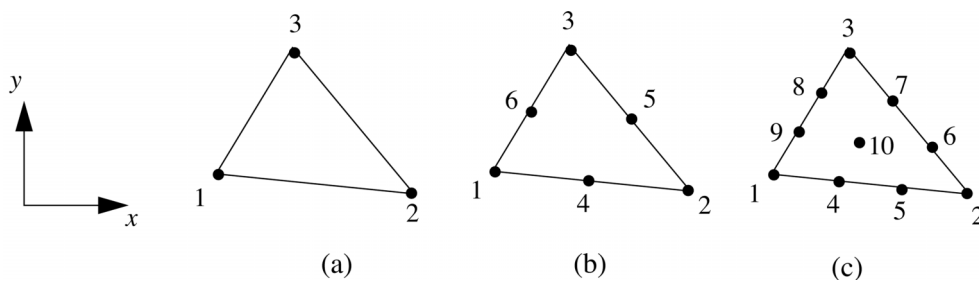


Fig. 1 Unconstrained and constrained elements' nodal configuration. (a) $N = 3$, Linear; (b) $N = 6$, Quadratic; (c) $N = 10$, Cubic

Table 1 Displacement interpolation for unconstrained and constrained elements

Element type	Unconstrained element	Constrained element
Degree of interpolation fields $w; \theta_x, \theta_y$	$(p + 1); p$	$(p + 1); p$
Degree of shear strain along s $\gamma_{sz} = w_{,s} + \theta_n$	p	$p - 1$
Number of nodes $N = (p + 1)(p + 2)/2$	N	N
Number of nodal DOF	$3N$	$3N$
Number of hierarchical DOF	$p + 2$	0
Number of constraint equations	0	$p + 2$

4.2 Unconstrained element interpolation

The nodal displacements of the N -node element are w_i , θ_{xi} and θ_{yi} , $i = 1, 2, \dots, N$, with

$$\mathbf{w} = \{w_i\} \quad \boldsymbol{\theta}_x = \{\theta_{xi}\} \quad \boldsymbol{\theta}_y = \{\theta_{yi}\} \quad (6a)$$

The vector of nodal degrees-of-freedom is

$$\mathbf{d} = \begin{Bmatrix} \mathbf{w} \\ \boldsymbol{\theta}_x \\ \boldsymbol{\theta}_y \end{Bmatrix} \quad (6b)$$

The standard Lagrange-type, p -degree interpolation functions, N_i , $i = 1, 2, \dots, N$, that are used extensively for plane triangular elements and that can be found in many finite element texts (see, e.g., Cook *et al.* 2002) are used for the rotations and for the transverse displacement. Because the transverse displacement is interpolated with functions of degree $p + 1$, hierarchical functions are used for the $p + 2$ higher-order terms. These functions, which are zero at the nodes, are most easily defined similar to the N_i , i.e., as products of linear functions passing through the nodes. The nodeless degrees-of-freedom associated with the hierarchical terms are represented by

$$\mathbf{a} = \{\bar{a}_j\}, \quad j = 1, 2, \dots, (p + 2) \quad (7)$$

The displacement interpolation can be expressed as

$$\mathbf{u} = \begin{Bmatrix} w \\ \theta_x \\ \theta_y \end{Bmatrix} = \begin{bmatrix} \mathbf{N} & \mathbf{0} & \mathbf{0} & \mathbf{N}_a \\ \mathbf{0} & \mathbf{N} & \mathbf{0} & \mathbf{0} \\ \mathbf{0} & \mathbf{0} & \mathbf{N} & \mathbf{0} \end{bmatrix} \begin{Bmatrix} \mathbf{w} \\ \boldsymbol{\theta}_x \\ \boldsymbol{\theta}_y \\ \mathbf{a} \end{Bmatrix} = \mathbf{N}_u \mathbf{d}_u \quad (8)$$

in which \mathbf{N} is the $1 \times N$ vector of the N_i and \mathbf{N}_a is the $1 \times (p + 2)$ vector of hierarchical interpolation

functions N_{aj} , $j = 1, 2, \dots, (p + 2)$. Note that the unconstrained elements have $3N$ nodal degrees-of-freedom and $p + 2$ nodeless degrees-of-freedom.

The unconstrained interpolation functions for MIN3, MIN6, and MIN10 are, respectively,

$$N_i = \xi_i \quad N_{ai} = \xi_i \xi_k \quad (9a)$$

$$N_i = \xi_i(2\xi_i - 1) \quad N_{i+3} = 4\xi_i \xi_k \quad N_{ai} = \xi_i \xi_k(2\xi_i - 1) \quad N_{a4} = \xi_1 \xi_2 \xi_3 \quad (9b)$$

and

$$\begin{aligned} N_i &= \frac{1}{2} \xi_i(3\xi_i - 1)(3\xi_i - 2) & N_{2i+2} &= \frac{9}{2} \xi_i \xi_k(3\xi_i - 1) & N_{2i+3} &= \frac{9}{2} \xi_i \xi_k(3\xi_k - 1) \\ N_{10} &= 27 \xi_1 \xi_2 \xi_3 & N_{ai} &= \xi_i \xi_k(3\xi_i - 1)(3\xi_i - 2) & N_{a4} &= \xi_1 \xi_2 \xi_3(3\xi_1 - 1) \\ & & N_{a5} &= \xi_1 \xi_2 \xi_3(3\xi_2 - 1) & & \end{aligned} \quad (9c)$$

with $i = 1, 2, 3$; $k = 2, 3, 1$ and the ξ_i are area coordinates.

4.3 Shear constraint equations

The tangential transverse shear γ_{sz} along any arbitrary line L that makes an angle α with the x -axis (Fig. 2) is defined as

$$\gamma_{sz} = w_{,s} + \theta_n \quad (10a)$$

in which θ_n is the midsurface-normal rotation as depicted. The relation between γ_{sz} , γ_{xz} and γ_{yz} is

$$\gamma_{sz} = \gamma_{xz} \cos \alpha + \gamma_{yz} \sin \alpha \quad (10b)$$

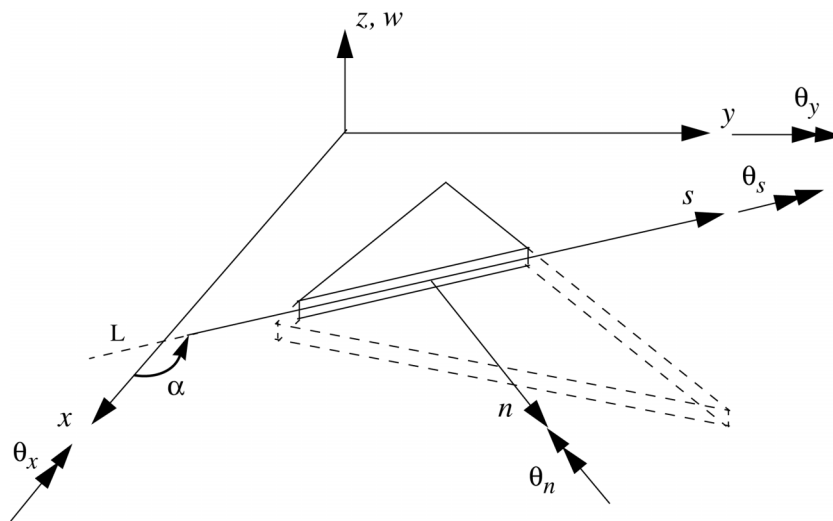


Fig. 2 Notation for MIN-N element

Our desired element, MIN- N , is obtained from the unconstrained element by eliminating the $p + 2$ nodeless degrees-of-freedom, \mathbf{a} , for which $p + 2$ constraints are needed. The $p + 2$ constraint equations are obtained from

$$\underbrace{\gamma_{sz,s\dots ss}}_p \equiv 0 \quad (11)$$

Eq. (11) says that the p -th partial derivative of the shear strain γ_{sz} along any direction is required to be zero. For example, for a 3-node element, $p = 1$ and the first partial derivative has to be zero; for a 6-node element, $p = 2$ and the second partial derivative has to be zero; etc. Although this high-order constraint reduces the degree of completeness of the shear strain polynomial by one, it is chosen because it 1) maintains interelement compatibility and 2) results in the highest degree shear strain field possible for the constrained element.

Eqs. (10b) and (11) result, for arbitrary α , in the $p + 2$ constraints

$$\begin{aligned} \frac{\partial^p \gamma_{xz}}{\partial x^p} &= 0 \\ (p-m) \frac{\partial^p \gamma_{xz}}{\partial x^{p-(m+1)} \partial y^{m+1}} + (m+1) \frac{\partial^p \gamma_{yz}}{\partial x^{p-m} \partial y^m} &= 0 \quad m = 0, 1, 2, \dots, (p-1) \\ \frac{\partial^p \gamma_{yz}}{\partial y^p} &= 0 \end{aligned} \quad (12)$$

To provide some clarity to Eq. (12), we state them explicitly for the first three members of the MIN- N family.

1. MIN3 is a 3-node triangle with $p = 1$, a quadratic displacement field, and linear rotation fields. The three constraint equations are

$$\gamma_{xz,x} = 0, \quad \gamma_{xz,y} + \gamma_{yz,x} = 0, \quad \gamma_{yz,y} = 0 \quad (13a)$$

2. MIN6 is a 6-node triangle with $p = 2$, a cubic displacement field, and quadratic rotation fields. The four constraint equations are

$$\gamma_{xz,xx} = 0, \quad 2\gamma_{xz,xy} + \gamma_{yz,yy} = 0, \quad \gamma_{xz,yy} + 2\gamma_{yz,xy} = 0, \quad \gamma_{yz,yy} = 0 \quad (13b)$$

3. MIN10 is a 10-node triangle with $p = 3$, a quartic displacement field, and cubic rotation fields. The five constraint equations are

$$\begin{aligned} \gamma_{xz,xxx} = 0, \quad 3\gamma_{xz,xy} + \gamma_{yz,xxx} = 0, \quad 2\gamma_{xz,xy} + 2\gamma_{yz,xy} = 0, \\ \gamma_{xz,yyy} + 3\gamma_{yz,xy} = 0, \quad \gamma_{yz,yyy} = 0 \end{aligned} \quad (13c)$$

4.4 Constrained interpolations

From Eqs. (2), (8), and (12), we can write the $(p + 2)$ constraints in terms of the nodal and nodeless degrees-of-freedom:

$$[\mathbf{0} \quad \mathbf{B}_{c\theta_x} \quad \mathbf{B}_{c\theta_y} \quad \mathbf{B}_{ca}] \begin{Bmatrix} \mathbf{w} \\ \theta_x \\ \theta_y \\ \mathbf{a} \end{Bmatrix} = \mathbf{0} \quad (14)$$

in which the \mathbf{B} matrices involve partial derivatives of the interpolation functions. From Eq. (14), the nodeless degrees-of-freedom \mathbf{a} can be written in terms of the nodal degrees-of-freedom because \mathbf{B}_{ca} is an invertible matrix. As a result, \mathbf{a} can be eliminated from Eq. (8), resulting in

$$\mathbf{u} = \mathbf{N}_c \mathbf{d} \quad (15a)$$

in which

$$\mathbf{N}_c = \begin{bmatrix} \mathbf{N} & \mathbf{L} & \mathbf{M} \\ \mathbf{0} & \mathbf{N} & \mathbf{0} \\ \mathbf{0} & \mathbf{0} & \mathbf{N} \end{bmatrix} \quad (15b)$$

\mathbf{N}_c is the $3 \times 3N$ matrix of constrained interpolation functions for MIN- N elements and

$$\mathbf{L}^T = \{L_i\} \quad \mathbf{M}^T = \{M_i\} \quad i = 1, 2, \dots, N \quad (15c)$$

L_i and M_i have degree $p+1$, one order higher than \mathbf{N} . Notice that as a result of enforcing the continuous shear constraints along any line in the element, the transverse displacements are now coupled to the bending rotations. (Note that when $\mathbf{L} = \mathbf{M} = \mathbf{0}$, the interpolation functions for the isoparametric family of elements are recovered.)

To guarantee that rigid body motions can be represented, the interpolation functions must satisfy the conditions

$$\sum_{i=1}^N N_i \equiv 1 \quad \sum_{i=1}^N L_i \equiv 0 \quad \sum_{i=1}^N M_i \equiv 0 \quad (16)$$

The restriction on N_i is clearly satisfied because these are the standard interpolation functions. The unconstrained interpolation functions certainly can represent rigid body motions. The constrained interpolation functions are obtained from the unconstrained functions by restricting the variation of the shear strains. Because rigid body motions involve zero shear, the constraints do not affect the ability of the constrained functions to represent rigid body motion, and hence the remaining two of Eq. (16) also will be satisfied.

Once the interpolation functions of MIN- N are developed, formulating the element stiffness, consistent mass matrices and consistent load vectors follows the straightforward procedure in the displacement-based finite element formulation. Stiffness, consistent mass matrices and consistent load vectors are obtained with full integration. We note that the strain-displacement matrices are

$$\mathbf{B}_b = \begin{bmatrix} \mathbf{0} & \mathbf{0} & N_{,x} \\ \mathbf{0} & N_{,y} & \mathbf{0} \\ \mathbf{0} & N_{,x} & N_{,y} \end{bmatrix} \quad (16a)$$

$$\mathbf{B}_s = \begin{bmatrix} \mathbf{N}_{,x} & \mathbf{L}_{,x} & \mathbf{M}_{,x} + \mathbf{N} \\ \mathbf{N}_{,y} & \mathbf{L}_{,y} + \mathbf{N} & \mathbf{M}_{,y} \end{bmatrix} \quad (16b)$$

The consistent mass matrix is

$$\mathbf{M} = \int_A \mathbf{N}_c^T \bar{\mathbf{m}} \mathbf{N}_c dA \quad (17)$$

in which $\bar{\mathbf{m}}$ is the 3×3 sectional mass matrix, including rotary inertia.

The consistent load vector for the distributed normal load, q , as well as applied bending moments, \bar{M}_{xx} , \bar{M}_{yy} , and transverse shear force, \bar{Q} , prescribed on the portion Γ_σ of the element boundary Γ may be written as

$$\mathbf{F} = \int_A q [\mathbf{N} \ \mathbf{L} \ \mathbf{M}]^T dA + \int_{\Gamma_\sigma} [\mathbf{0} \ \bar{M}_{yy} \mathbf{N} \ \bar{M}_{xx} \mathbf{N}]^T d\Gamma + \int_{\Gamma_\sigma} \bar{Q} [\mathbf{N} \ \mathbf{L} \ \mathbf{M}]^T d\Gamma \quad (18)$$

4.5 Shear variation of MIN-N

The transverse shear strains in the unconstrained elements are complete polynomials of degree p . The shear constraints limit the shear strain variation for MIN-N. To satisfy the first and last shear constraints in Eq. (12), the shear strains must be of the form

$$\gamma_{xz} = \sum_{n=0}^{p-1} \left(\sum_{m=0}^n A_{n-m,m} x^{n-m} y^m \right) + \sum_{m=1}^p A_{p-m,m} x^{p-m} y^m \quad (19a)$$

$$\gamma_{yz} = \sum_{n=0}^{p-1} \left(\sum_{m=0}^n B_{n-m,m} x^{n-m} y^m \right) + \sum_{m=0}^{p-1} B_{p-m,m} x^{p-m} y^m \quad (19b)$$

in which the coefficients A and B involve the nodal degrees-of-freedom. (The subscript notation is such that the comma separates the two indices and does not imply differentiation, and repeated indices do not imply summation.) Satisfaction of the other p constraint equations requires

$$A_{p-n-1,n+1} + B_{p-n,n} = 0 \quad n = 0, 1, \dots, p-1 \quad (20)$$

4.6 Kirchhoff constraints of MIN-N

In the thin plate regime as $L/t \rightarrow \infty$, the Kirchhoff constraints, Eq. (3), are enforced over the entire element domain. Together with Eqs. (19a), (19b) and (20), we obtain

$$A_{n-m,m} (A_{p-n-1,n+1} = -B_{p-n,n}), B_{n-m,m} \rightarrow 0 \quad m = 0, 1, \dots, n; \quad n = 0, 1, \dots, p-1 \quad (21)$$

These are the $p \times (p+2)$ Kirchhoff constraint equations for MIN-N in the thin plate limit.

Although the formulation here is somewhat different and has been generalized for higher-order elements, it can be readily verified (Liu 2002) that the interpolation functions and constraint equations, when specialized for $N = 3$, are the same as for the original MIN3 element as given in (Tessler 1985, Tessler and Hughes 1985).

5. Formulation of MIN6

The 6-node, 18 degree-of-freedom (DOF) element MIN6 is developed based on the general formulation of MIN- N . Fig. 1(b) shows the nodal configuration for MIN6, and the unconstrained interpolation functions are given in Eq. (9b).

5.1 Constrained interpolation functions

The constrained interpolation functions are obtained from the unconstrained interpolation functions by imposition of the 4 shear constraints in Eq. (13b). Note that the interpolation functions are defined in terms of the area coordinates ξ_i rather than in terms of x and y , and therefore the derivatives needed in Eq. (13b) are not immediately available. If the element is distorted (i.e., the edges are curved), the Jacobian matrix is not constant, and the resulting constrained interpolation functions would not be polynomials because of the inverse of \mathbf{B}_{ca} , and the nodeless degrees-of-freedom \mathbf{a} would not be constant. Hence, a straight sided element is assumed in the derivation of the interpolation functions. As a result, the linear relation between Cartesian and area coordinates for a straight-sided triangle is valid:

$$\xi_i = \frac{1}{2A}(c_i + b_i x + a_i y) \quad (22a)$$

in which coefficients a_i , b_i , and c_i are given by

$$a_i = x_k - x_j \quad b_i = y_j - y_k \quad c_i = x_j y_k - x_k y_j \quad (22b)$$

with a cyclic permutation of the indices ($i = 1, 2, 3; j = 2, 3, 1; k = 3, 1, 2$). x_i and y_i are the nodal coordinates of node i . Although this assumption does not necessarily restrict the actual element geometry to be straight-sided, it is anticipated that MIN6's performance will be sensitive to distortion (i.e., to the placement of the middle nodes).

The constrained interpolation functions in terms of the area-parametric coordinates, \mathbf{N}_c , can be obtained as

$$N_i = \xi_i(2\xi_i - 1) \quad N_{i+3} = 4\xi_i\xi_k \quad (22c)$$

$$L_i = N_i \frac{1}{3}(b_k \xi_j - b_j \xi_k) \quad L_{i+3} = N_{i+3} \frac{1}{3} \left[b_i \xi_k - b_k \left(\xi_i - \frac{1}{2} \right) \right] \quad (22d)$$

$$M_i = -N_i \frac{1}{3}(a_k \xi_j - a_j \xi_k) \quad M_{i+3} = -N_{i+3} \frac{1}{3} \left[a_i \xi_k - a_k \left(\xi_i - \frac{1}{2} \right) \right] \quad (22e)$$

with $i = 1, 2, 3; j = 2, 3, 1; k = 3, 1, 2$. It is readily verified that the conditions for rigid body motions, Eq. (16), are satisfied by these functions.

5.2 Kirchhoff constraints of MIN6

The 8 Kirchhoff constraints in the thin limit can be obtained generally from Eq. (20). However, there is an alternative formulation of these constraints. Consider the element in Fig. 1(b). Along any edge ij , the transverse displacement, $w(s)$, is a cubic function and the edge-normal rotation, $\theta_n(s)$, is a quadratic function in terms of the edge coordinate s . Imposition of the Kirchhoff constraint, Eq. (10a) leads to two Kirchhoff edge constraints per edge, for a total of six ‘edge’ constraints:

$$\frac{1}{2}(w_i + w_j) - w_{i+3} + \frac{1}{8}[b_k(\theta_{xi} - \theta_{xj}) - a_k(\theta_{yi} - \theta_{yj})] = 0 \tag{23a}$$

$$3(w_i - w_j) + \frac{1}{2}[b_k(\theta_{xi} + \theta_{xj} + 4\theta_{xi+3}) - a_k(\theta_{yi} + \theta_{yj} + 4\theta_{yi+3})] = 0 \tag{23b}$$

with a cyclic permutation of the indices.

From Eq. (21) we know there are 8 Kirchhoff constraints. We refer to the remaining two as ‘interior’ constraints. To find them, first consider Fig. 1(b) again. Imagine lines connecting each vertex node with the opposite midside node. Along each of these lines, the Kirchhoff constraint can be imposed, resulting in the ‘interior’ Kirchhoff constraints:

$$7(w_i - w_k) + 10(w_{j+3} - w_{i+3}) + (a_k - a_j)(\theta_{yi} - \theta_{yj+3}) - (b_k - b_j)(\theta_{xi} - \theta_{xj+3}) + (a_j - a_i)(\theta_{yi+3} - \theta_{yk}) + (b_j - b_i)(\theta_{xi+3} - \theta_{xk}) = 0 \tag{24}$$

again with a cyclic permutation of the indices. Eq. (24) represents three equations, only two of which are independent (any two can be used).

The 8 Kirchhoff constraints of MIN6 are given explicitly in Eqs. (23a), (23b) and (24). Specific details of the derivation can be found in Liu (2002).

When 4 MIN6 elements are placed in a cross-diagonal pattern, as depicted in Fig. 3, one would expect to have 24 Kirchhoff constraints (2 per edge plus 2 per element). However, it can be shown that there are only 23 independent constraints. One can therefore expect better performance in the thin limit for MIN6 when used in a cross-diagonal meshing scheme, as compared to the

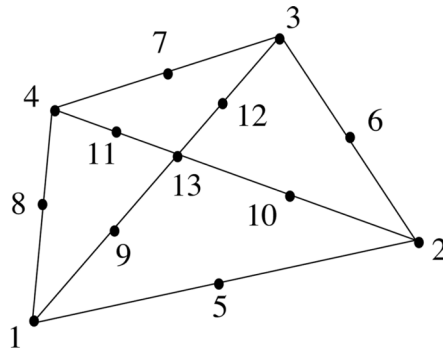


Fig. 3 MIN6 cross-diagonal pattern

performance in other meshing schemes. Conceptually, one obtains an additional ‘free’ degree-of-freedom in each pattern by the elimination of one constraint. (The same is true for MIN3.) Hence, this cross-diagonal meshing strategy is used in most of the test problems discussed below.

Remark. The smoothing element analysis methodology for stress recovery and *a posteriori* error estimation for finite element analysis has been developed recently; see, e.g., (Riggs *et al.* 1997, Tessler *et al.* 1998, 1994, Yazdani *et al.* 2000). The method results in a nearly C^1 continuous recovered stress field based on the underlying interelement-discontinuous finite element stress field. The method can result in a superconvergent recovered stress field if the smoothing element is of sufficient order relative to the finite element stresses. In the cited work, the interpolation functions and constraint equations for MIN3 were used to develop a quadratic smoothing element, which is most effective when applied to finite element stress fields that are linear within the finite element. Higher order smoothing elements are recommended for higher order finite elements. The interpolation functions and constraint equations developed herein allows the development of higher order smoothing elements.

6. Numerical results for MIN6

MIN6 can reproduce rigid body modes when the element is both undistorted (straight edges) and distorted (curved edges). It passes the thin plate, constant moment patch test proposed by MacNeal and Harder (1985) when the element is undistorted, but not when it is curved. This is clearly a result of the related assumption in the development of the interpolation functions; see the discussion in section 5.1. As a result, only straight-sided elements are used subsequently. The same mesh proposed in MacNeal and Harder (1985) was used here, except that each quadrilateral was meshed by two triangles. In addition, MIN6 passes the mixed patch tests involving constant moment and linear moment involving a tip-loaded cantilever ‘beam’ described in Batoz and Lardeur (1989).

An important factor in the performance of MIN3, especially for coarse meshes, is the element-appropriate shear relaxation. Tests were carried out to determine if MIN6 required shear relaxation, and it was shown that the element does not (Liu 2002). None of the results presented herein involves relaxation; i.e., $\phi^2 \equiv 1$ for all cases.

6.1 Thin limit behavior

To evaluate the performance of MIN6 in the thin limit, a series of analyses involving square, simply supported and clamped plates subjected to a concentrated center load and a uniform distributed load were carried out. The L/t ratio was varied from 10 to 1000. For comparison, results are compared to those for a 6-node, displacement-based, isoparametric Mindlin plate element with full integration (ISOMIN6). ISOMIN6 has the same formulation as MIN6, except that $\mathbf{L} = \mathbf{M} = \mathbf{0}$. Clearly, the element has the same nodal configuration as that of MIN6. The three meshes shown in Fig. 4 were used. Center displacements, nondimensionalized by the Kirchhoff solutions, are plotted for MIN6 and ISOMIN6 in Figs. 5 and 6. The results show that MIN6 neither locks nor is excessively stiff, even for thin plates and the coarse 2×2 meshes. However, ISOMIN6 results with the 2×2 coarse mesh show clearly that the element has substantially poorer performance for thin plates, and locks completely for the clamped plate.

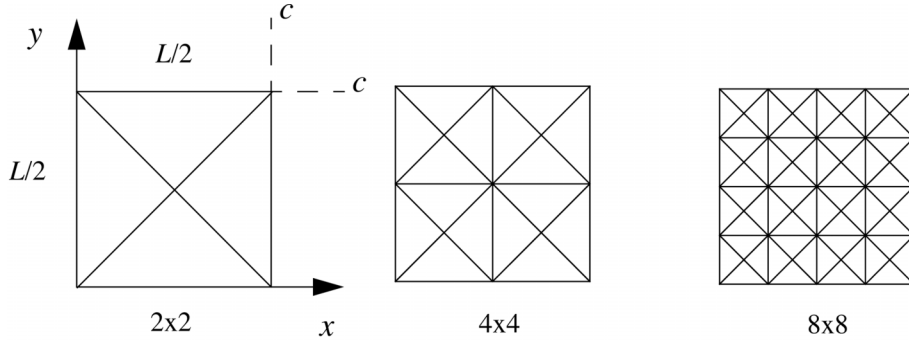


Fig. 4 Meshes of one quadrant of a symmetric, square plate

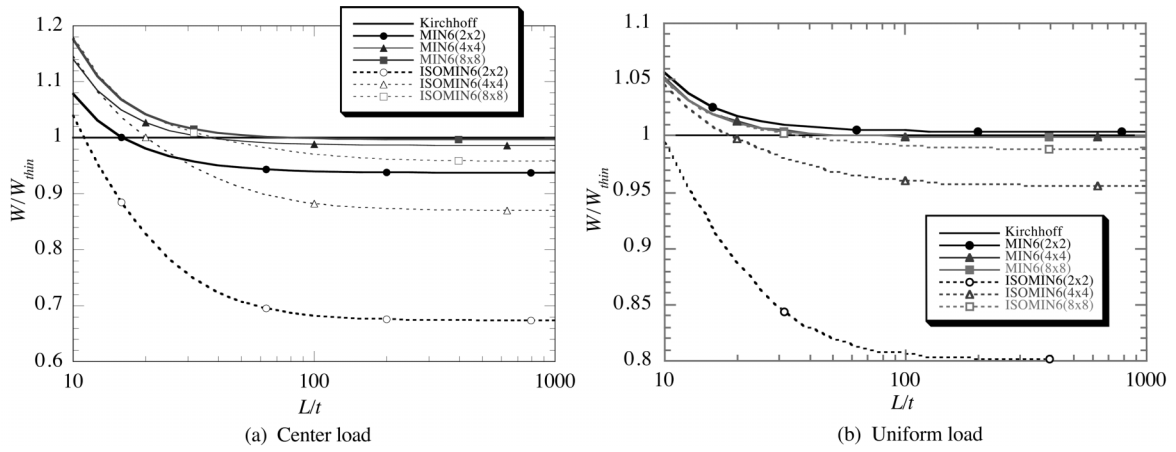


Fig. 5 Center displacement of a simply supported plate with varying L/t ratios and three meshes

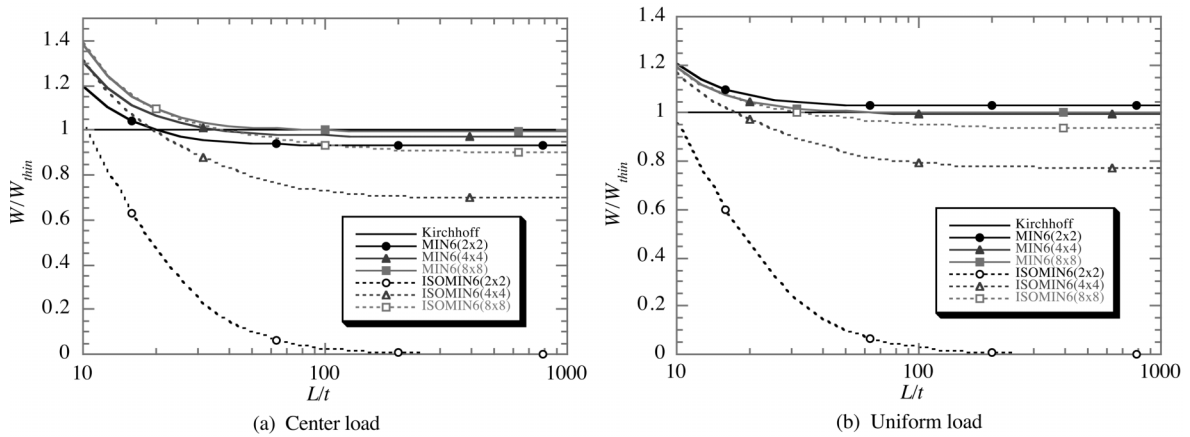


Fig. 6 Center displacement of a clamped plate with varying L/t ratios and three meshes

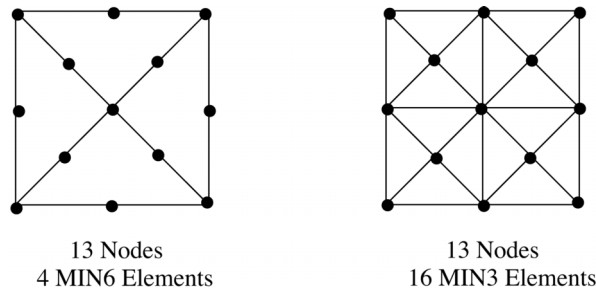


Fig. 7 The cross-diagonal meshes of MIN6 and MIN3 for plate problems

6.2 Meshing strategy

In the subsequent tests, results for MIN6 are compared with MIN3 and ANSYS' SHELL93 (ANSYS 1998) element. SHELL93 was chosen as an example of a commercially-available, 6-node triangle. SHELL93 is a reduced-integrated, isoparametric element with a shear relaxation factor, which is conceptually similar to ϕ^2 , to prevent shear locking.

The preferred meshing strategy for both MIN6 and MIN3 is a cross diagonal pattern, as depicted in Fig. 7. The figures shows a basic quadrilateral meshed with the same nodal pattern for both MIN6 and MIN3. SHELL93 meshes are identical to the MIN6 meshes (This configuration may not be optimal for SHELL93.) Meshes for all three elements therefore have the same number of nodes and degrees-of-freedom. Note that the MIN3 meshes have four times the number of elements as the MIN6 meshes.

6.3 Isotropic thin and moderately thick square plates ($L/t = 1000$ and 10)

Convergence studies are carried out for a thin square plate with L/t of 1000 and a moderately thick square plate with L/t of 10. Simply supported and clamped boundary conditions are used, and the plates are subjected to a uniform load and a center concentrated load. The meshes are shown in Fig. 8. Poisson's ratio is 0.3 in all cases. The center deflection and center bending moment were chosen to evaluate the numerical performance. Fourier series solutions, which are used to

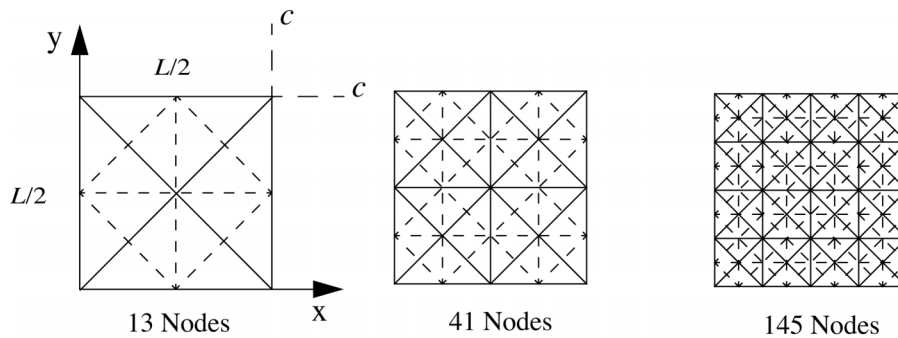


Fig. 8 One quadrant of doubly-symmetric square plates (dashed lines indicate MIN3 elements)

nondimensionalize the results, are given in Table 2. W_{thin} and M_{thin} (Liu *et al.* 2000) are Kirchhoff theory solutions of the center deflection and bending moment and W_{mind} are Mindlin theory solutions of the center deflection. P is the center point load, q is the uniform load, and $D = Et^3/12(1 - \nu^2)$, where E and ν are Young's modulus and Poisson's ratio, respectively.

Table 2 Reference solutions for center deflection and bending moment of a square plate

Boundary condition and loading	Square plate		
	W_{thin}	W_{mind}	M_{thin}
Simply supported with center load	$0.0116PL^2/D$	----	----
Clamped with center load	$0.00560PL^2/D$	---	----
Simply supported with uniform load	$0.00406qL^4/D$	$0.00427qL^4/D$	$0.0479qL^2$
Clamped with uniform load	$0.00126qL^4/D$	$0.00150qL^4/D$	$0.0231qL^2$

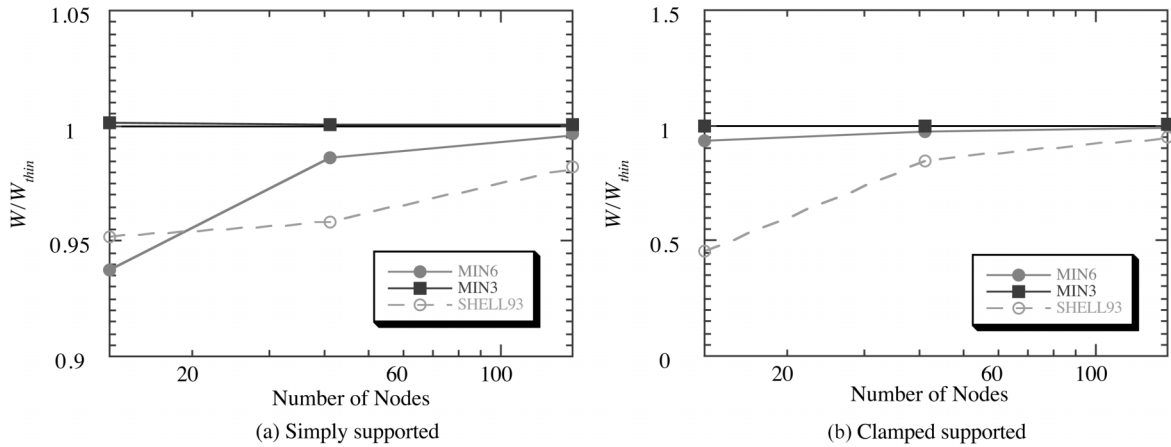


Fig. 9 Convergence of center deflection for a thin square plate with center load

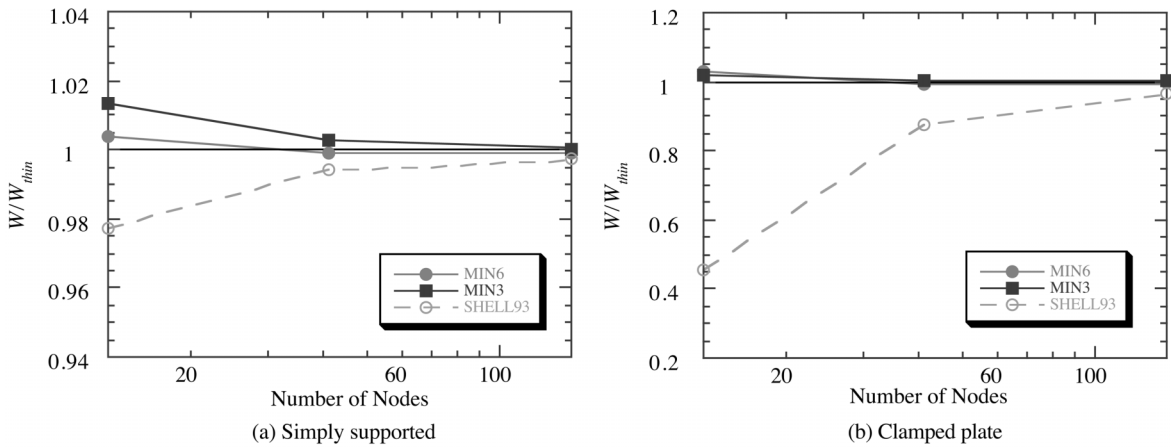


Fig. 10 Convergence of center deflection for thin square plate with uniform load

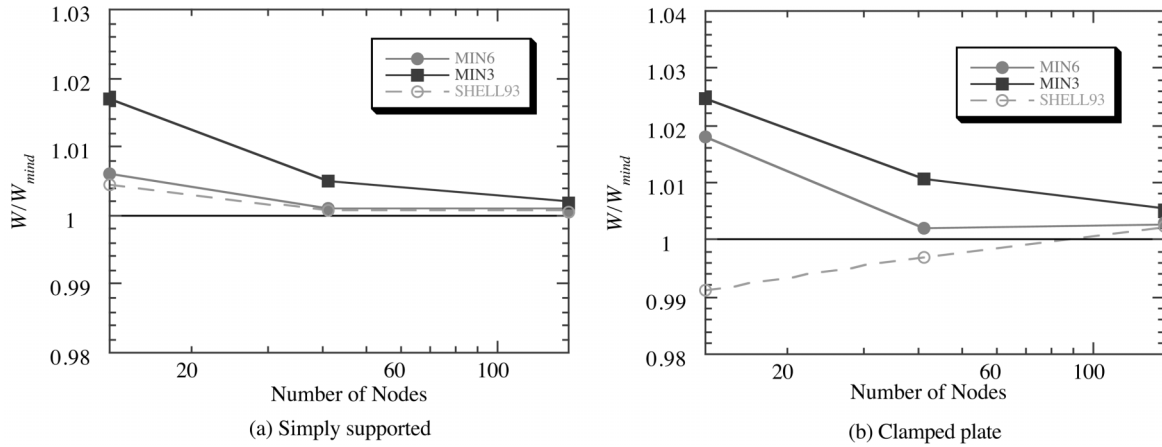


Fig. 11 Convergence of center deflection for moderately thick square plate with uniform load

Convergence plots are shown in Figs. 9 to 11. The results show that MIN6 is as accurate as MIN3 and in some cases more accurate. Both elements are more accurate than SHELL93. All elements, however, illustrate convergent behavior. Note that in Fig. 9 MIN3 displays greater accuracy than MIN6. This is because the shear relaxation factor ϕ^2 for MIN3 has been optimized based on this problem, i.e., a thin square plate with a concentrated load.

For the fine meshes, the errors in the center moments for MIN6, as measured by the averages of the moments at the integration points closest to the center of the plate, were 0.5% and 1.7% for the simply supported and clamped plates, respectively.

6.4 Thin circular plates ($2R/t = 100$)

A simply-supported, thin circular plate ($2R/t = 100$) is used to demonstrate the performance of MIN6 when nonrectangular 4-element assemblies are used. The three meshes shown in Figs. 12 and 13 are used. MIN6 and SHELL93 have the same meshes and MIN3's meshes are shown in Fig. 13.

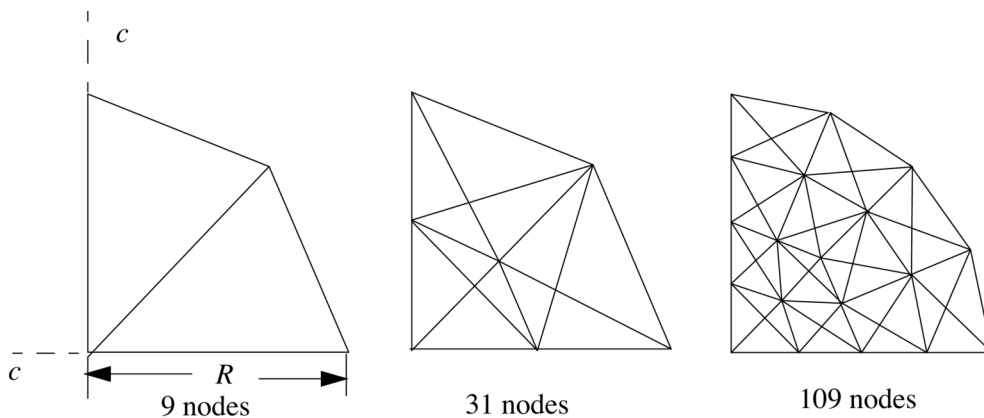


Fig. 12 MIN6 and SHELL93 meshes for 1/4 thin circular plate

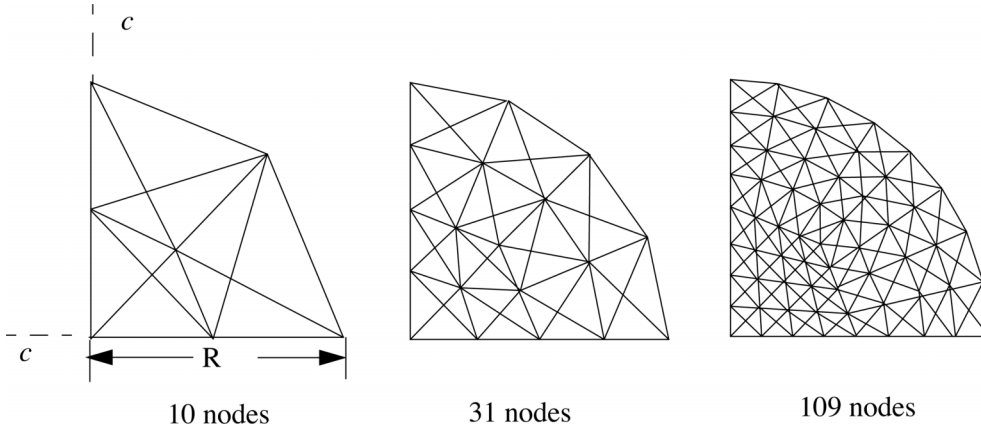


Fig. 13 MIN3 meshes for 1/4 thin circular plate

Table 3 Exact solutions for center deflection and bending moment of a circular plate (Roark and Young 1975)

Boundary condition and loading	W_{thin}	M_{thin}
Simply supported with center point load	$PR^2(3 + \nu)/[16\pi D(1 + \nu)]$	----
Simply supported with uniform load	$qR^4(5 + \nu)/[64D(1 + \nu)]$	$qR^2(3 + \nu)/16$

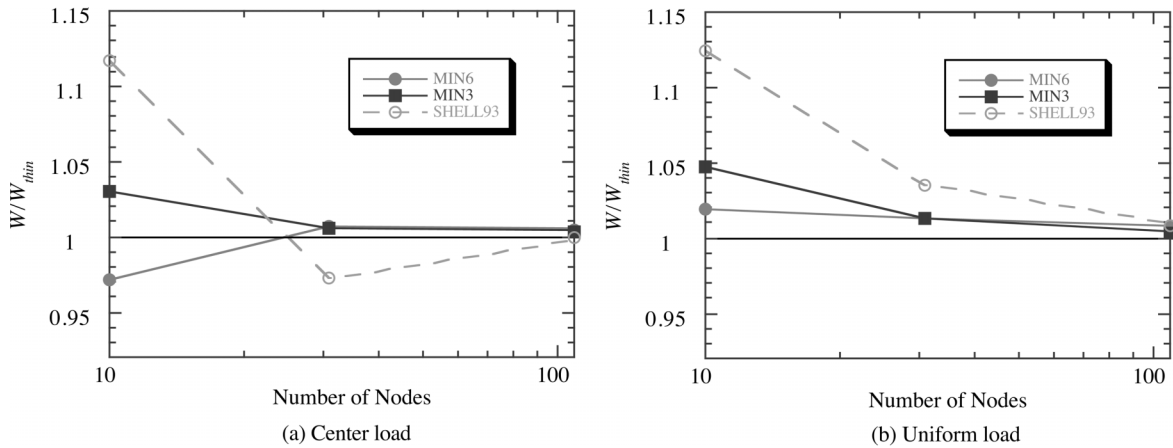


Fig. 14 Convergence of center deflection for thin circular plate ($2R/t = 100$)

To keep MIN6 straight-sided, only the element's vertex nodes are placed on the circular boundary. Only the transverse displacement of the nodes on the circular plate boundary are restrained. Poisson's ratio is 0.3. Center deflection results, as a ratio of the exact solutions in Table 3, are shown in Fig. 14. MIN6's performance is excellent for deflection in the thin regime, and the element competes well with MIN3 and SHELL93.

For the fine mesh, MIN6's center moment, based on the average of the moments at the closest integration points, is in error by less than 0.1%.

6.5 Orthotropic square plate ($L/t = 30$)

A simply supported, orthotropic thin square plate ($L/t = 30$) is used to test the convergence and accuracy of MIN6 for non-isotropic problems. The meshes are shown in Fig. 8. Material properties are $E_x = 22.9 \times 10^6$; $E_y = E_z = 1.39 \times 10^6$; $G_{xy} = G_{xz} = 0.86 \times 10^6$; $G_{yz} = 0.468 \times 10^6$; $\nu_{xy} = \nu_{xz} = 0.32$ and $\nu_{yz} = 0.49$. (These properties correspond to a Gr/Ep unidirectional composite.) A uniform sine loading, $q = \sin(\pi x/L)\sin(\pi y/L)$, is applied. The load within each triangle of the finite element model varied quadratically for MIN6 and linearly for MIN3. Convergence of the center deflection, bending moments and shear forces are shown in Figs. 15 to 18. For comparison, exact solutions (Liu *et al.* 2000) and the results of MIN3 are presented in the figures. MIN6's results are excellent. For MIN6 and MIN3, the bending moments and shear forces are obtained from the Gauss point closest to the corner or edges.

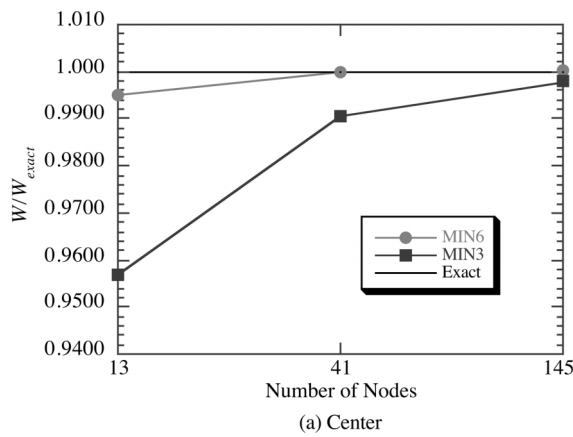


Fig. 15 Convergence for center deflection of orthotropic square plate ($L/t = 30$)

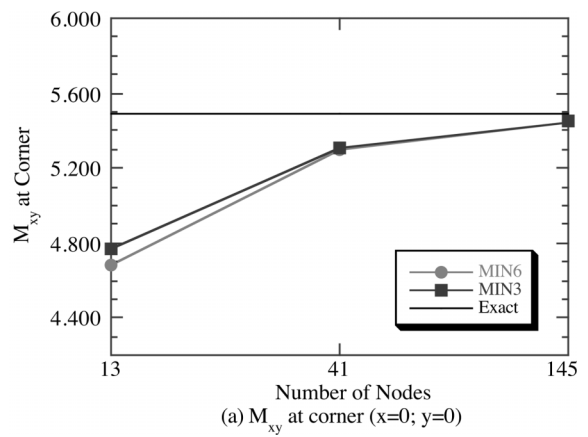


Fig. 16 Convergence of moment M_{xy} of orthotropic square plate ($L/t = 30$)

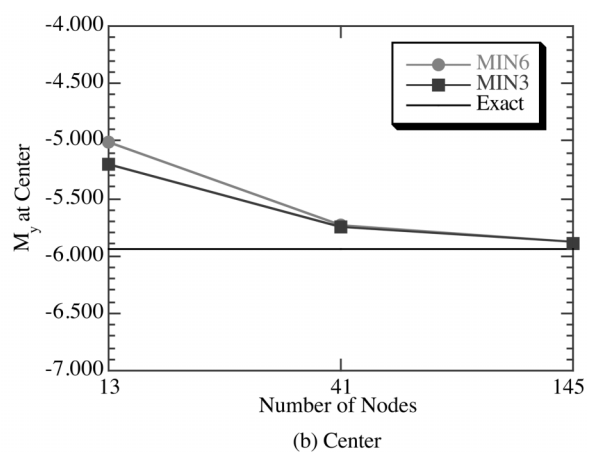
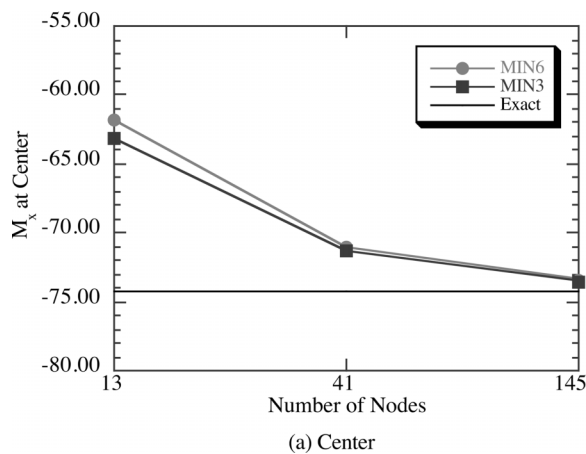


Fig. 17 Convergence of moment M_x and M_y of orthotropic square plate ($L/t = 30$)

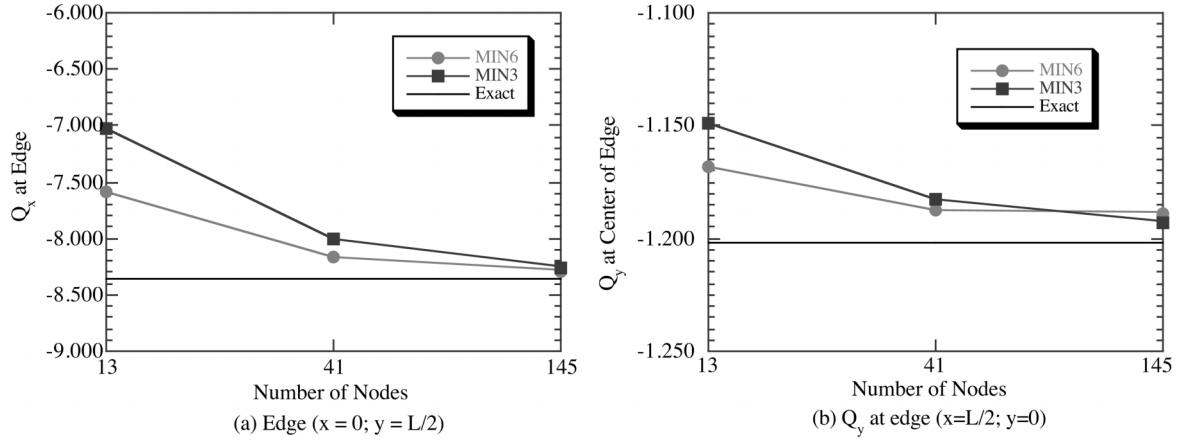


Fig. 18 Convergence of shear force Q_x and Q_y of orthotropic square plate ($L/t = 30$)

6.6 Thin rhombic (skew) plate

A thin, simply-supported rhombic plate with an acute angle of 30° is frequently used to test plate elements. A '4 × 4' mesh of 16 MIN6 elements is shown in Fig. 19. The corresponding MIN3 mesh with the same number of DOFs has 64 elements. The plate was given properties of $a = 100$, $t = 1$, $E = 1 \times 10^7$ and $\nu = 0.3$ (Ibrahimbegovic and Frey 1994). The plate has a uniformly

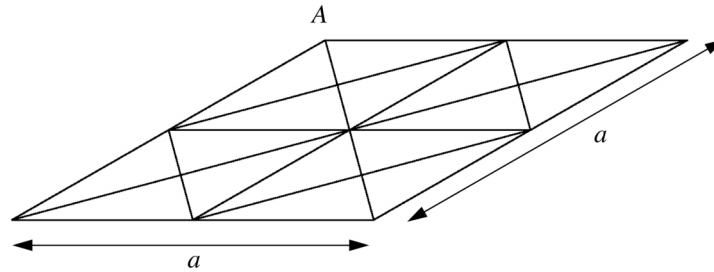


Fig. 19 '4 × 4' MIN6 mesh of a rhombic plate

Table 4 Center displacements and moments for the skew plate

Mesh	$\frac{w}{qa^4/1000D}$		$\frac{M_{max}}{qa^2/100}$		$\frac{M_{min}}{qa^2/100}$	
	MIN6	MIN3	MIN6	MIN3	MIN6	MIN3
4 × 4	0.443	0.466	1.81	1.78	1.04	0.982
8 × 8	0.395	0.430	1.84	1.90	1.07	1.10
16 × 16	0.410	0.422	1.91	1.93	1.10	1.12
Reference	0.408	0.408	1.91	1.91	1.08	1.08

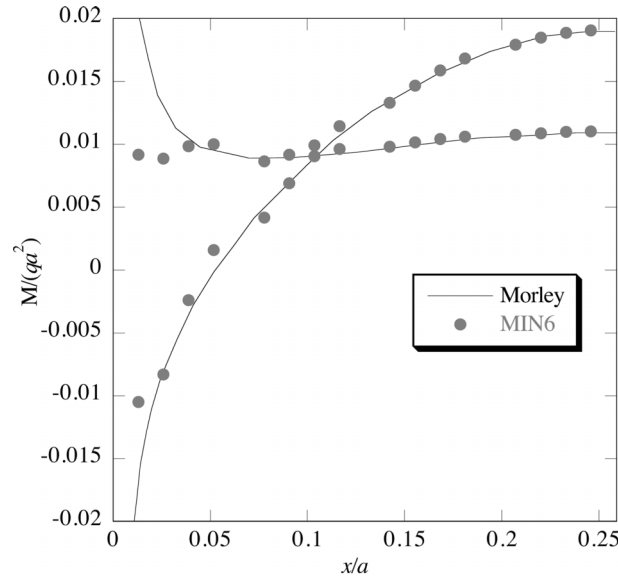


Fig. 20 Bending moments along short diagonal

distributed load of magnitude q . Transverse displacement and principal moments at the center of the plate for 3 meshes (4×4 , 8×8 , and 16×16) are given in Table 4. The reference solution is from Morley (1963). The moments along the short diagonal, from point A to the plate center in Fig. 19, are shown in Fig. 20 for the 16×16 mesh. The moments for MIN6 are obtained from the integration points closest to the line (two per element). It is clear that MIN6 performs very well, having difficulty only near the singularity at A.

6.7 Free vibration of thin and moderately-thick plates

The natural frequencies of simply-supported thin ($L/t = 10^4$) and moderately thick ($L/t = 10$) isotropic square plates have been computed with the 64 element mesh (145 nodes) shown in Fig. 8. Poisson's ratio is 0.3. The exact, Mindlin-solution nondimensional frequencies $\lambda_{nm} = \omega_{nm} L^2 \sqrt{\rho/(Et^2)}$ (where ω_{nm} is the natural frequency for mode m, n and ρ is the mass density) for the symmetric modes are presented in Table 5 (Liu *et al.* 1998). The percent error of the frequencies are shown in Table 6

Table 5 Non-dimensional frequencies λ_{nm} for simply-supported square plates exact solutions (Liu *et al.* 2000)

Mode number		Thin plate ($L/t = 10^4$)	Thick plate ($L/t = 10$)
		λ_{nm}	λ_{nm}
n	m	Mindlin	Mindlin
1	1	5.97337	5.76932
1	3	29.8668	25.7337
3	3	53.7602	42.3832

Table 6 Percent error in frequencies λ_{nm} for simply-supported square plates

Mode number		Thin plate ($L/t = 10^4$)		Thick plate ($L/t = 10$)	
		% error in λ_{nm}		% error in λ_{nm}	
n	m	MIN6	MIN3	MIN6	MIN3
1	1	0.0256	-0.1746	0.0196	-0.1518
1	3	1.2787	0.2350	0.6605	0.7830
3	3	1.8094	-1.0835	1.3666	1.0389

for MIN6 and MIN3. Consistent mass matrices with full integration were used for both elements. Rotary inertia was included with MIN6 (the MIN3 element does not include rotary inertia). The results demonstrate the good performance of MIN6. The pure displacement formulation and full integration implementation of MIN6 leads to the expected consistent overestimation of each natural frequency. Note that because of the shear relaxation factor for MIN3, the element is not a 'pure' displacement element and it does not always predict an upper bound on the frequencies.

A more detailed analysis of the element's performance for free vibration problems appears in Liu and Buchanan (2004). Numerical results are compared with experimental data and previously published numerical results. The results for MIN6 compare very favorably.

7. Conclusions

A general derivation for the interpolation functions of a family of higher-order, pure-displacement, triangular Mindlin plate elements is developed. The development has been motivated by the successful performance of MIN3 (Tessler and Hughes 1985), which becomes the lowest order element in the family. The transverse displacement is interpolated by a polynomial one order higher than the interpolation of the rotations. The transverse displacement is coupled with the bending rotations by enforcing continuous shear constraints along any line in the element. The elements possess fully compatible kinematic fields.

An efficient, cubic-displacement, compatible, fully-integrated, six-node element, MIN6, with neither shear locking nor excessive stiffness in the thin limit, is generated as an example of a higher-order element in the family. MIN6 has the straightforward formulation and implementation characteristic of pure, displacement-based elements. Based on numerical testing, MIN6 is accurate and robust when it is straight-sided. For meshes with the same number of degrees-of-freedom, it is comparable in accuracy to MIN3 and the ANSYS' SHELL93 (ANSYS 1998) element. In addition, MIN6 does not require shear relaxation in the thin limit. Extension of the element to a flat shell element is straightforward.

As a result of the assumption of a straight-sided triangle in developing the interpolation functions, MIN6 does not pass the constant-moment patch test when the sides are curved, and therefore at present it should only be used as a strict triangle. To extend the applicability of the element, methods should be explored to improve its performance with curved sides.

References

- ANSYS. (1998), *Ansys User's Manual*, v. 5.5.
- Auricchio, F. and Taylor, R.L. (1994), "A shear deformable plate element with an exact thin limit", *Comput. Meth. Appl. Mech. Eng.*, **118**, 393-412.
- Bathe, K.J., Brezzi, F. and Cho, S.W. (1989), "The MITC7 and MITC9 plate bending element", *Comput. Struct.*, **32**, 797-814.
- Bathe, K.J. and Dvorkin, E.N. (1985), "A four-node plate bending element based on Mindlin/Reissner plate theory and a mixed interpolation", *Int. J. Num. Meth. Eng.*, **21**, 367-383.
- Batoz, J.L. (1982), "An explicit formulation for an efficient triangular plate-bending element", *Int. J. Num. Meth. Eng.*, **18**, 1077-1089.
- Batoz, J.L. and Lardeur, P. (1989), "A discrete shear triangular nine d.o.f. element for the analysis of thick to very thin plates", *Int. J. Num. Meth. Eng.*, **28**, 533-560.
- Belytschko, T., Stolarski, H. and Carpenter, N. (1984), "A C^0 triangular plate element with one-point quadrature", *Int. J. Num. Meth. Eng.*, **20**, 787-802.
- Belytschko, T. and Wong, B.K. (1989), "Assumed strain stabilization procedure for the 9-node Lagrange shell element", *Int. J. Num. Meth. Eng.*, **28**, 385-414.
- Brezzi, F., Bathe, K.J. and Fortin, M. (1989), "Mixed-interpolated elements for Reissner/Mindlin plates", *Int. J. Num. Meth. Eng.*, **28**, 1787-1801.
- Choi, C.K. and Park, Y.M. (1999), "Quadratic NMS Mindlin-plate-bending element", *Int. J. Num. Meth. Eng.*, **46**, 1273-1289.
- Cook, R.D., Malkus, D.S., Plesha, M.E. and Witt, R.J. (2002), *Concepts and Applications of Finite Element Analysis*, John Wiley & Sons.
- Crisfield, M.A. (1984), "A quadratic Mindlin element using shear constraints", *Comput. Struct.*, **18**(5), 833-852.
- Crisfield, M.A. (1986), *Finite Elements and Solution Procedures for Structural Analysis*, Pineridge Press, Swansea, U.K.
- de Veubeke, B.F. (1965), "Displacement and equilibrium models in the finite element method", in *Stress Analysis: Recent Developments in Numerical and Experimental Methods*, O.C. Zienkiewicz and G.S. Holister, eds., John Wiley & Sons, London, 145-197.
- Greimann, L.F. and Lynn, P.P. (1970), "Finite element analysis of plate bending with transverse shear deformation", *Nucl. Eng. Des.*, **14**, 223-230.
- Hughes, T.J.R. and Cohen, M. (1978), "The 'heterosis' finite element for plate bending", *Comput. Struct.*, **9**, 445-450.
- Hughes, T.J.R., Taylor, R.L. and Kanoknukulchai, W. (1977), "A simple and efficient finite element for plate bending", *Int. J. Num. Meth. Eng.*, **11**, 1529-1543.
- Hughes, T.J.R. and Tezduyar, T.E. (1981), "Finite elements based upon Mindlin plate theory with particular reference to the four-node bilinear isoparametric element", *J. Appl. Mech.*, **48**, 587-596.
- Ibrahimbegovic, A. and Frey, F. (1994), "Stress resultant geometrically non-linear shell theory with drilling rotations. Part III: Linearized kinematics", *Int. J. for Numerical and Analytical Methods in Geomechanics*, **37**, 3659-3683.
- Liu, J., Riggs, H.R. and Tessler, A. (2000), "A four-node, shear-deformable shell element developed via explicit Kirchhoff constraints", *Int. J. Num. Meth. Eng.*, **49**(8), 1065-1086.
- Liu, Y.J. (2002), "Development of the MIN-N family of triangular anisoparametric Mindlin plate elements", Ph.D. dissertation, University of Hawaii at Manoa, Honolulu.
- Liu, Y.J. and Buchanan, G.R. (2004), "Free vibration of stepped cantilever Mindlin plates", *J. Sound Vib.*, **271**, 1083-1092.
- Liu, Y.J., Riggs, H.R. and Tessler, A. (1998), "A 4-node anisoparametric Mindlin plate element based on the Tessler 3-node element", *UHM/CE/98-01*, University of Hawaii at Manoa, Honolulu.
- MacNeal, R.H. (1978), "A simple quadrilateral shell element", *Comput. Struct.*, **8**, 175-183.
- MacNeal, R.H. (1982), "Derivation of element stiffness matrices by assumed strain distributions", *Nucl. Eng. Des.*, **70**, 3-12.
- MacNeal, R.H. and Harder, R.L. (1985), "A proposed standard set of problems to test finite element accuracy",

- Finite Elem. Anal. Design*, **1**, 3-20.
- Morley, L.S.D. (1963), *Skew Plates and Structures*, MacMillan, New York.
- Pugh, E.D.L., Hinton, E. and Zienkiewicz, O.C. (1978), "A study of quadrilateral plate bending elements with 'reduced' integration", *Int. J. Num. Meth. Eng.*, **12**, 1059-1079.
- Riggs, H.R., Tessler, A. and Chu, H. (1997), " C^1 -continuous stress recovery in finite element analysis", *Comput. Meth. Appl. Mech. Eng.*, **143**(3/4), 299-316.
- Roark, R.J. and Young, W.C. (1975), *Formulas for Stress and Strain*, McGraw-Hill Book Company, New York.
- Sheikh, A.H. and Dey, P. (2001), "A new triangular element for the analysis of thick and thin plates", *Comm. Num. Meth. Engr.*, **17**, 667-673.
- Sze, K.Y. (1997), "Quadratic triangular C^0 plate bending element", *Int. J. Num. Meth. Eng.*, **40**, 937-951.
- Sze, K.Y. and Zhu, D. (1998), "A quadratic assumed natural strain triangular element for plate bending analysis", *Comm. Num. Meth. Engr.*, **14**, 1013-1025.
- Taylor, R.L. and Auricchio, F. (1993), "Linked interpolation for Reissner-Mindlin plate elements: Part II. A simple triangle", *Int. J. Num. Meth. Eng.*, **36**, 3057-3066.
- Tessler, A. (1982), "On a conforming, Mindlin-type plate element", in *The Mathematics of Finite Elements and Applications IV*, J.R. Whiteman, ed., Academic Press, London, 119-126.
- Tessler, A. (1985), "A priori identification of shear locking and stiffening in triangular Mindlin elements", *Comput. Meth. Appl. Mech. Eng.*, **53**(2), 183-200.
- Tessler, A. (1990), "A C^0 -anisoparametric three-node shallow shell element", *Comput. Meth. Appl. Mech. Eng.*, **78**, 89-103.
- Tessler, A. and Dong, S.B. (1981), "On a hierarchy of conforming Timoshenko beam elements", *Comput. Struct.*, **14**(3-4), 335-344.
- Tessler, A. and Hughes, T.J.R. (1983), "An improved treatment of transverse shear in the Mindlin-type four-node quadrilateral element", *Comput. Meth. Appl. Mech. Eng.*, **39**, 311-335.
- Tessler, A. and Hughes, T.J.R. (1985), "A three-node Mindlin plate element with improved transverse shear", *Comput. Meth. Appl. Mech. Eng.*, **50**, 71-101.
- Tessler, A., Riggs, H.R., Freese, C.E. and Cook, G.M. (1998), "An improved variational method for finite element stress recovery and *a posteriori* error estimation", *Comput. Meth. Appl. Mech. Eng.*, **155**, 15-30.
- Tessler, A., Riggs, H.R. and Macy, S.C. (1994), "A variational method for finite element stress recovery and error estimation", *Comput. Meth. Appl. Mech. Eng.*, **111**, 369-382.
- Xu, Z. (1992), "A thick-thin triangular plate element", *Int. J. Num. Meth. Eng.*, **33**, 963-973.
- Yazdani, A.A., Riggs, H.R. and Tessler, A. (2000), "Stress recovery and error estimation for shell structures", *Int. J. Num. Meth. Eng.*, **47**, 1825-1840.
- Zienkiewicz, O.C. and Lefebvre, D. (1988), "A robust triangular plate bending element of the Reissner-Mindlin type", *Int. J. Num. Meth. Eng.*, **26**, 1169-1184.
- Zienkiewicz, O.C., Xu, Z., Zeng, L.F., Samuelsson, A. and Wiberg, N.E. (1993), "Linked interpolation for Reissner-Mindlin plate elements: Part I. A simple quadrilateral", *Int. J. Num. Meth. Eng.*, **36**, 3043-3056.